Flow condensation heat transfer of CO_2 in a horizontal tube at low temperatures

Peihua Li[a], J.J.J. Chen[b], Stuart Norris[a*]

[a]Department of Mechanical Engineering

[b]Department of Chemical and Materials Engineering

The University of Auckland, Auckland 1142, New Zealand

[*]Corresponding author.

Tel.: +6499239625

Fax: +6493737479

Email: s.norris@auckland.ac.nz

Address: Engineering Block 1, Level 7, Room 401-703, 20 Symonds Street, Auckland, New Zealand

Abstract

This study presents experimental data of CO_2 flow condensation heat transfer for mass fluxes ranging from 100 to 500 kg/m^2-s inside a 4.73 mm inside diameter, smooth horizontal copper tube, at saturation temperatures between -10 to 0˚C under a wide range of vapour quality conditions. Experimental data were obtained from an open-loop test rig which discharged high-pressure CO_2 liquid from bottles to the atmosphere. Experimental results showed that when the test mass flux was greater than or equal to 300 kg/m^2-s, for vapour qualities greater than 0.4, the rate of heat transfer increased with increasing mass flux and vapour quality, and increased with decreasing saturation temperature. The flow regimes under these working conditions were predicted as annular from the values of the Soliman Froude number ($Fr_{so} > 14$). Three recently proposed CO_2 flow condensation models from the open literature were evaluated against the data from the current experiment. The model of Li and Norris [2016] had the best overall prediction but under-predicted the low Nusselt number heat transfer data. This model was modified and re-evaluated against experimental data from the current and other experiments, and was found to have a mean absolute percentage deviation of 7%.

Keywords

Carbon dioxide, flow condensation, heat transfer coefficient, low temperatures

1. Introduction

Carbon dioxide (R744, CO_2) is a natural refrigerant that is increasingly being used in the low-temperature circuit of cascade and secondary refrigeration systems. Its main advantage over existing synthetic refrigerants is its environmental friendliness, having a low greenhouse warming potential, being non-toxic and non-ozone depleting. In addition, CO_2 has been stated as the most efficient and effective volatile secondary refrigerant, due to the significantly reduced primary refrigerant charge required, resulting in a high system efficiency and a low required pumping power [2]. A number of experimental studies have been conducted to date so as to better understand the heat transfer characteristics of CO_2 flow boiling and condensation, and to provide engineers with suitable models for the design of evaporators and condensers used in cascade or secondary systems [3-10].

While there have been numerous studies of flow boiling [9, 10], information about CO_2 flow condensation is still limited. A recent review by the current authors showed that there are inconsistencies in the experimental data of CO_2 flow condensation from different studies at similar working conditions [11]. More specifically, the dependency of the measured heat transfer coefficient (HTC) on changes in the vapour quality x, mass flux G and saturation temperature T_{sat}, differed among the experimental studies, as listed in Table.1. In addition, existing generic models of flow condensation developed from data of other refrigerants typically over-predict the experimental heat transfer coefficients for CO_2, due to its unique thermophysical properties at high reduced-pressure conditions. The high thermal conductivity, enthalpy of vaporisation and specific heat of CO_2 are outside of the range of validity for the existing correlations. There is a need to be able to accurately predict the rate of heat transfer in CO_2 flow condensation, since inside cascade condensers, CO_2 flow condensation has a heat transfer resistance of similar magnitude to the resistance on the other side of condensers, which correspond to the flow boiling of the high-temperature stage refrigerant.

Effects of variation of working conditions on heat transfer	**Zilly et al.[3] Jang and Hrnjak [4]** (i.d.* 6.1mm)	**Kim et al. [5]** (i.d. 3.48mm)	**Iqbal and Bansal [7]** (i.d. 6.52mm)	**Kang et al. [12]** (i.d. 5.15mm)
***x* (range from 0.2 to 0.8)**	HTC increase of 115% at G=400kg/m^2-s T_{sat}=-15˚C	HTC increase of 103% at G=400kg/m^2-s T_{sat}=-15˚C	HTC increase of 40% at G=200kg/m^2-s T_{sat}=-15˚C	HTC increase of 7% at G=600kg/m^2-s T_{sat}=-10˚C
***G* (*x*= 0.8)**	HTC increase of 63% from 200 to 400kg/m^2-s at T_{sat}=-15˚C	HTC increase of 150% from 200 to 800kg/m^2-s at T_{sat}=-15˚C	HTC increase of 32% from 50 to 200kg/m^2-s at T_{sat}=-15˚C	HTC increase of 4% from 600 to 1000kg/m^2-s at T_{sat}=-10˚C
***T*$_{sat}$ (*x*= 0.8)**	HTC increase of 17% from -25 to -15˚C at 400kg/m^2-s	HTC increase of 15% from -25 to -15˚C at 800kg/m^2-s	HTC increase of 19% from -15 to -5˚C at 200kg/m^2-s	HTC increase of 6% from -10 to 0˚C at 600kg/m^2-s
Corresponding mass flux for HTC from 2000 to 6000W/m^2-K	200 to 400kg/m^2-s at **T_{sat}=-15˚C**	200 to 400kg/m^2-s at **T_{sat}=-15˚C**	50 to 200kg/m^2-s at **T_{sat}=-15˚C**	600 to 1000kg/m^2-s at **T_{sat}=-15˚C**

*** i.d.: Inside diameter**

Table 1. A comparison of the dependence of heat transfer on mass flux and saturation temperature, as found from different experimental studies[11]

To supplement the limited and inconsistent data in the open literature, this study reports measurements of CO_2 flow condensation heat transfer inside a horizontal, 4.73 mm inside diameter smooth copper tube for mass fluxes ranging from 100 to 500 kg/m^2-s at low saturation temperatures of -10 to 0°C. The heat transfer characteristics were analysed in terms of the effects of the mass flux, vapour quality and saturation temperature on the heat transfer coefficient.

The present experimental data were used to evaluate three flow condensation models which have been specifically proposed for CO_2 [1, 13, 14]. The accuracy of the models is presented in terms of the mean percentage deviation σ_a and the mean absolute percentage deviation σ_b, as used by other authors [15, 16],

$$\sigma_a = \frac{1}{N}\sum \frac{Nu_{predicted} - Nu_{measured}}{Nu_{measured}} \times 100$$
$$\sigma_b = \frac{1}{N}\sum abs\left(\frac{Nu_{predicted} - Nu_{measured}}{Nu_{measured}}\right) \times 100 \quad (1)$$

Heo and Yun [13] proposed a model which they compared against seven different sources of experimental data with a mean absolute percentage deviation of 44.8%. However, the mean percentage deviations between the predictions and different experimental studies are inconsistent. Shah [14] examined one of his own flow condensation correlations [17] and found it performed satisfactorily for CO_2 flow condensation for mass fluxes less than 300 kg/m^2-s with a mean absolute percentage deviation of 22.7%. Shah also noted that existing correlations poorly predicted the heat transfer data for mass fluxes greater than 300 kg/m^2-s. Li and Norris [1] developed a model using published data sources [3-6] selected on the repeatability and consistency of the data for each study. Their total prediction was acceptable with a mean absolute percentage deviation of 7.7%. Based on a comparison against the experimental data presented in this study, the Li and Norris model is modified to improve its accuracy for the prediction of CO_2 flow condensation heat transfer.

2. The experimental test rig

A schematic of the open-loop test rig used is shown in Fig.1, with the main components listed in Table.2. High pressure (55 bar) liquid CO_2 is initially drawn from the storage bottles (1) and is eventually discharged into the atmosphere (1 bar). The mass flow rate of the CO_2 fluid, which is measured by a Coriolis mass flow meter (3), is controlled by the flow coefficient of a throttling valve (4) and the set pressure of a back pressure regulator (8). There are two baths (9 and 11) which stabilise the temperature of the low-temperature e-glycol water mixture provided by the chiller (10).

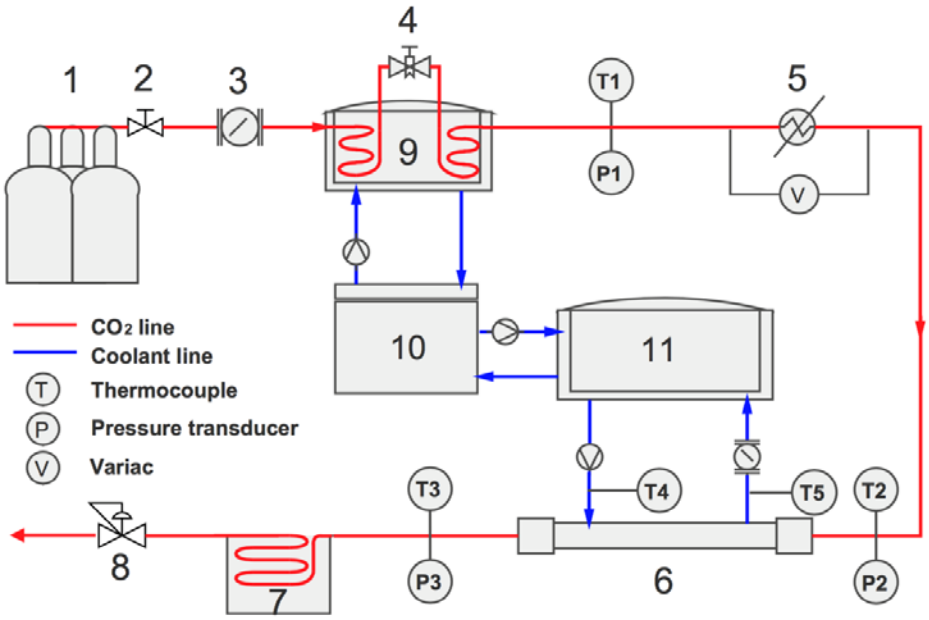

Figure 1. A schematic drawing of the open-loop experimental rig

Index	Description	Supplier	Part Number	Main parameters
1	**CO_2 Storage bottle**	BOC Gas	GE169	Quantity:3 30 kg/bottle liquid CO_2
2	**Shutoff valve**	Swagelok	SS-4PDM4-F4	69 bar at 121°C
3	**Coriolis mass flow meter**	Yokogawa	RCCS31	Uncertainty: 0.1%
4	**Metering valve**	Swagelok	SS-4MG	Flow coefficient up to 0.03
5	**Preheater**	-	-	Refer to Fig.4 Heating capacity: 3 kW
6	**Test section**	-	-	Refer to Fig.3
7	**Post-heater**	-	-	-
8	**Back pressure regulator**	Swagelok	KPB1L0A415P2 0000	Flow coefficient: 0.2
9	**Internal circulating bath**	Thermo Fisher	AC200, 1560021	Temperature stability: ±0.01°C
10	**Main refrigeration unit**	Thermo Fisher	ULT95, 179104241600	Temperature stability: ±0.2°C, Cooling capacity: 750 W at -30°C
11	**External circulating bath**	Thermo Fisher	AC200, 1560021	Temperature stability: ±0.01°C

Table 2. The main components of the open-loop experimental rig

After being discharged from the bottles, the CO_2 fluid is initially pre-cooled inside the internal circulating bath (9), where the internal temperature is maintained at -25°C. This pre-cooling process is illustrated in the pressure-enthalpy (*P-h*) diagram Fig.2a, with the frictional pressure drop of CO_2 fluid ignored for reasons of clarity. The pre-cooled liquid CO_2 is then throttled by the metering valve (4) and changes to two-phase flow as its saturation pressure P_{sat} drops to the set pressure (26.5 bar in Fig.2) of the back pressure regulator (8), shown in Fig.2b. Due to this throttling process, the CO_2 two-phase flow obtains sufficient kinetic energy to flow through the rest of test rig. After valve (4), the two-phase CO_2 enters into the constant temperature bath (9) to be sub-cooled, shown in Fig.2c. This process is to allow the determination of the enthalpy of the CO_2 fluid before the preheater (5) from the measured temperature T_1 and pressure P_1 of the fluid.

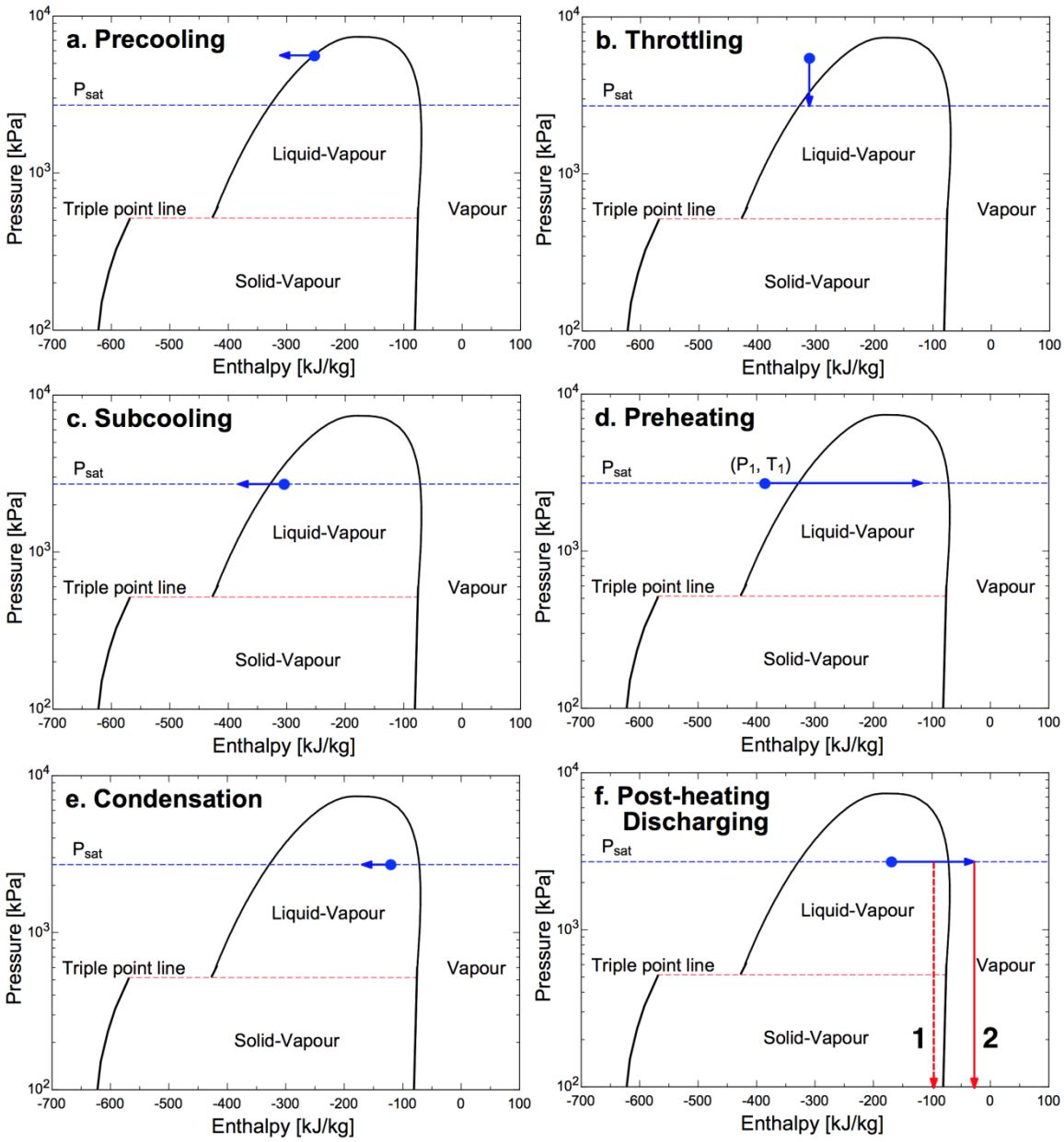

Figure 2. Changes in the state of the CO_2 fluid at a saturation pressure P_{sat} of 26.5 bar inside the test rig illustrated on the Pressure-Enthalpy diagram. For clarity the frictional pressure drop has been neglected.

The preheater (5) works by applying an adjustable low-voltage and high-amperage electric current to a stainless steel pipe coil, which works as a resistance heater. The preheating process enables the setting of the desired vapour quality of the CO_2 two-phase flow at the inlet of the test section (6). In Fig.2d, the preheating process is represented with a starting point determined by T_1 and P_1, on the *P-h* diagram. A 1.5-meter long pipe after the preheater (5) serves as a calming section to stabilise the two-phase CO_2 fluid before it enters the test section for the measurement of condensation.

The test section (6) is a double-tube counter-flow heat exchanger with the coolant flowing through the outer annulus and the CO_2 fluid flowing inside the inner copper tube. The coolant is

pumped by the external circulating bath (11) to the test section, and its temperature increases from T_4 to T_5 by absorbing heat from the flowing CO_2 two-phase fluid. Fluctuations in the inlet temperature, and flow rate of the coolant, are minimised by use of the tempering bath (11) which ensures stable operating conditions. The state change of the CO_2 two-phase flow during the condensation measurement is illustrated in Fig.2e.

Downstream of the test section, the two-phase CO_2 enters the post-heater (7) and is super-heated. The super-heated CO_2 vapour then passes through the back pressure regulator (8) and is ultimately discharged into the outdoor ambient air. The post-heating and discharging processes are shown in Fig.2f. Because the static pressure of CO_2 drops below the triple-point pressure after the regulator (8), dry ice may form, represented by a vertical red dash-line (as indicated by line 1) intersecting the solid-vapour region in Fig.2f. Formation of dry ice blocks the pipework and can affect the stability of mass flow rate and the system pressure. To avoid the formation of dry ice, the end point of the post-heating process is kept sufficiently far from the saturated vapour line (as indicated by line 2) in Fig.2f. Therefore, the resulting pressure drop process from the system pressure P_{sat} to the atmosphere pressure occurs without intersecting the solid-vapour zone. This is done by using a sufficiently long section of pipework as a post-heater (7).

3. Data reduction

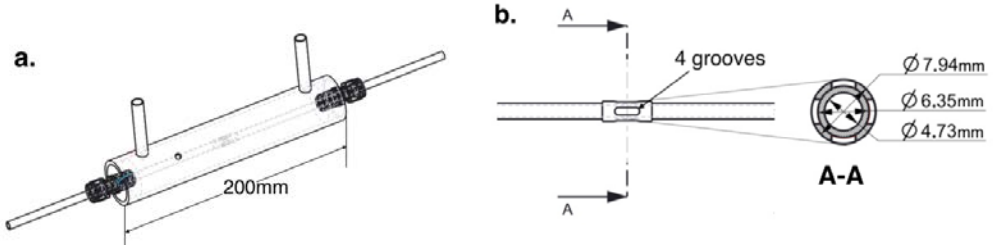

Figure 3. a. The double-tube heat exchanger test section. b. Detailed drawing of the temperature measurement location on the external tube wall.

The CO_2 condenses inside the inner tube of the double-tube heat exchanger test section labelled (6) in Fig.1, with the coolant flowing through the annulus formed with the outer tube, as shown in Fig.3a. The inner tube is made of copper, and has an inside diameter of 4.73 mm as shown in Fig.3b. The heat transfer coefficient for the CO_2 flow condensation in the test section is defined as,

$$h = \frac{\dot{Q}_{CO_2}}{A_{c,in}\left(T_{sat} - T_{w,in}\right)} \tag{2}$$

where $\dot{Q}_{CO_2}$ is the rate of heat transfer from the two-phase CO_2 flow to the coolant, $A_{c,in}$ is the inside surface area of the inner tube in the test section, and $T_{w,in}$ and T_{sat} are the inside surface temperature of the inner tube and the saturation temperature of the CO_2, respectively. As $T_{w,in}$ cannot be measured directly, it is calculated from,

$$T_{w,in} = \dot{Q}_{CO_2} R_{tube} + T_{w,out} \quad (3)$$

where R_{tube} is the conductive resistance of the inner tube and $T_{w,out}$ is the average surface temperature of the exterior surface of the inner tube. This temperature is measured using four thermocouples located in grooves evenly cut into the surface of a short sleeve tube, which is a snug fit to the outside of the inner tube in the test section (shown in Fig.3b). This ensures the thermocouples do not protrude into the thermal boundary layer of the coolant flowing in the outer tube, ensuring that the temperature of the external tube wall is accurately measured.

The rate of heat transfer to the coolant is calculated from the change in enthalpy of the coolant passing through the test section,

$$\dot{Q}_{coolant} = \dot{m}_{coolant} c_{p,coolant} (T_5 - T_4) \quad (4)$$

An energy balance on the test section requires that the heat transfer to the coolant, $\dot{Q}_{coolant}$, is equal to the sum of the heat transferred from the condensing CO_2, $\dot{Q}_{CO_2}$, the axial conduction along the tube containing the CO_2 into the test section, $\dot{Q}_{cond}$, and the heat gain from the surroundings through the test section insulation $\dot{Q}_{gain,test}$.

$$\dot{Q}_{coolant} = \dot{Q}_{CO_2} + \dot{Q}_{cond} + \dot{Q}_{gain,test} \quad (5)$$

An estimate of the magnitude of the axial conduction showed that its relative magnitude decreased with an increasing mass flow rate of the CO_2. Neglecting the axial conduction was estimated to introduce a maximum error of 5% at the lowest mass flux conditions, and so $\dot{Q}_{cond}$ was ignored in the data reduction. However, $\dot{Q}_{gain,test}$ was included in the analysis, and its measurement is discussed below in section 4.

The temperature and pressure of the sub-cooled liquid CO_2 flow are measured to determine the initial enthalpy of the fluid, i_1. The fluid is then preheated before entering the test section. The vapour quality of the two-phase CO_2 flow at the inlet of the test section x_{in}, is determined from the static pressure P_2 and the enthalpy i_2 calculated from an energy balance performed on the preheater,

$$i_2 = \left(\dot{E}_{pre} + \dot{Q}_{gain,pre}\right)/\dot{m}_{CO_2} + i_1 \quad (6)$$

The electric power input into the preheater $\dot{E}_{pre}$ is measured in real-time by a clamp meter, and $\dot{m}_{CO_2}$ is the measured CO_2 mass flow rate. The measurement of the heat gain of the flowing CO_2 from the surroundings in the preheater, $\dot{Q}_{gain,pre}$, is described in section 4 below.

The representative vapour quality x for the quasi-local heat transfer coefficient h is defined as the average value of vapour qualities at the inlet and outlet of the test section. The outlet vapour quality x_{out} is calculated from,

$$x_{out} = x_{in} - \frac{\dot{Q}_{CO_2}}{\dot{m}_{CO_2} i_{lv}} \tag{7}$$

where i_{lv} is specific enthalpy of vaporization of CO_2. Only partial condensation takes place and the maximum change in the vapour quality in the test section was 0.064 for the lowest mass flux (100 kg/m^2-s), so any possible subcooling of CO_2 may be ignored in this expression.

4. Determination of heat gain from the surroundings

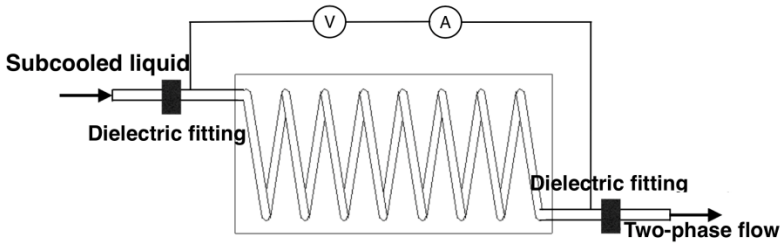

Figure 4. The schematic drawing of the preheater, labelled (5) in Fig.1

A detail of the preheater is shown in Fig.4. It consists of a 6-meter long stainless steel pipe coil with two dielectric fittings electrically isolating it from the rest of the rig. The pipe wall is used as a resistance heater, and is contained inside a vacuum cabinet, which is filled with nitrogen gas to avoid possible condensation within the cabinet. The use of a non-conducting cabinet ensures electrical isolation from the surroundings, to maintain electrical safety. An adjustable low-voltage, high-amperage current is applied to the pipe wall to heat the subcooled liquid CO_2 to a two-phase state.

The heat gain of the CO_2 flowing through the preheater from the surroundings, $\dot{Q}_{gain,pre}$, was determined through the measurement of a heat gain coefficient $(UA)_{pre}$. This measurement was determined from the heat transfer to sub-cooled single-phase liquid CO_2 flowing through the preheater when no electrical power was applied. The rate of heat gain was assumed to vary as,

$$\dot{Q}_{gain,pre} = (UA)_{pre} \Delta T_{logm,pre} = \dot{m}_{CO_2} c_{p,CO_2} (T_2 - T_1) \tag{8}$$

Measurement of the mass flow rate of the liquid CO_2, the inlet and outlet temperatures of the sub-cooled liquid CO_2 through the preheater, T_1 and T_2, knowledge of the specific heat of the liquid CO_2, and the calculation of the log-mean temperature difference between the CO_2 and the surroundings, $\Delta T_{logm,pre}$,

$$\Delta T_{logm,pre} = \big((T_{amb} - T_1) - (T_{amb} - T_2)\big) / \ln((T_{amb} - T_1)/(T_{amb} - T_2)) \tag{9}$$

allow the determination of $(UA)_{pre}$.

The total heat transfer resistance between the surroundings and the subcooled liquid CO_2 through the preheater insulation is,

$$\frac{1}{(UA)_{pre}} = R_{conv,in} + R_{cond,tube} + R_{cond,ins} + R_{conv,out} \tag{10}$$

The resistances $R_{conv,in}$, $R_{cond,tube}$, $R_{cond,ins}$ and $R_{conv,out}$ are the internal single-phase convection resistance of the CO_2 stream, the conduction resistance of the tube wall of the preheater, the conduction resistance of the insulation, and the convection resistance between the external insulation surface and the surroundings, respectively.

The Dittus-Boelter equation has that the convection heat transfer coefficient for single-phase turbulent flow in smooth tubes is related to the fluid velocity by $h \propto u^{0.8}$. Therefore, given that all the resistances remain unchanged, except $R_{conv,in}$, which will vary with the CO_2 mass flow rates, Eq.10 can be reduced to,

$$\frac{1}{(UA)_{pre}} = \frac{a}{u^{0.8}} + b \tag{11}$$

This linear relationship can be validated by determining $(UA)_{pre}$ for different mass flow rates. In Eq.11, $(UA)_{pre}$ is calculated from Eq.8 and u is from the measurement of the mass flow rate. The data points with Reynolds numbers of 2388, 4459 and 10316, are plotted in Fig.5, and Eq.11 was determined to be $1/(UA)_{pre} = 0.04/u^{0.8} + 1.35$(K/W).

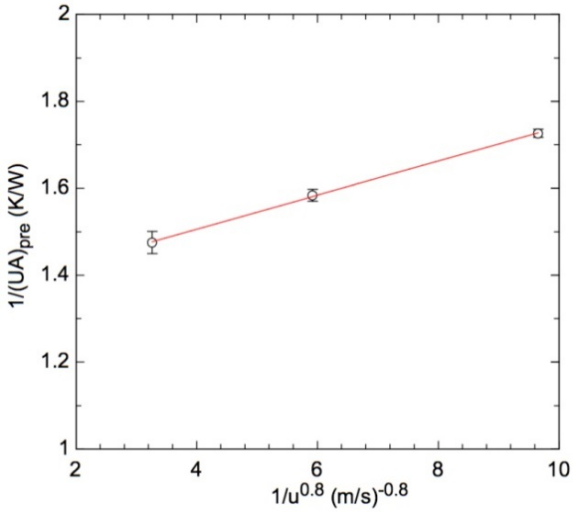

Figure 5. The linear relationship between $1/(UA)_{pre}$ and $1/u^{0.8}$ from Eq.11

It should be noted that the determination of the heat gain coefficient, $(UA)_{pre}$, has been made for single-phase liquid CO_2, and so an error can be assumed in applying the equation to a liquid undergoing phase change as will happen in the preheater. However, Fig.5 shows that the resistance of the heat gain from the preheater is dominated by $R_{cond,ins}$ and $R_{conv,out}$, since the intersection of the vertical axis much greater than zero, and so the value of $(UA)_{pre}$ from Eq.11

can be applied to the case when the heating of the liquid CO_2 involves heat transfer to both single and two-phase flow inside the preheater.

It should be pointed out that, the heat gain coefficient estimated above will no longer be accurate when the tube wall is heated, since as the electric power is increased, the temperature difference between the tube wall and the CO_2 fluid will increase, while that between the tube and the surroundings will decrease, thereby decreasing the heat gain from the surroundings. This will result in an overestimation of the heat gain from the ambient, with the error increasing as the power applied to the wall is increased. However, the correction has been used for the data processing, since for low values of electric heating the error in the correction is small, and the heat gain from the surroundings is significant, being approximately 10% of that provided by the electric heating. In contrast, for high values of electric heating, while the error in the estimation of the heat gain from the surroundings can be in error by approximately 30%, the heat gain from the surroundings is small in comparison with the electric heating, being on the order of 1% of the total heat gain of the CO_2, and so the error in using the above correction is minimal.

For the test section, the heat gain from the surroundings, $\dot{Q}_{gain,test}$ was assumed to vary as,

$$\dot{Q}_{gain,test} = (UA)_{test}\Delta T_{logm,test} \tag{12}$$

where $(UA)_{test}$ is the heat gain coefficient and $\Delta T_{logm,test}$ is the log-mean temperature difference between the coolant temperature in the test section heat exchanger, increasing from T_4 to T_5, and the ambient temperature of the surroundings, T_{amb}. In order to determine the value of $(UA)_{test}$ for test conditions, the flow rate of the coolant supplied to the test section was set to a fixed value for both the calibration and the experimental test runs. During the calibration, no CO_2 fluid passed through the test section. The inlet temperature of the coolant T_4 was set to different values, and the corresponding outlet temperatures T_5 were recorded after a settling time. The rate of heat gain was calculated from,

$$\dot{Q}_{gain,test} = \dot{m}_{coolant}c_{p,coolant}(T_5 - T_4) \tag{13}$$

Different calibration points are plotted in Fig.6, and a fit to Eq.13 is $\dot{Q}_{gain,test} = 0.075 + 0.48\Delta T_{logm,test}$(W). The heat gain coefficient of the test section $(UA)_{test}$ at the fixed coolant flow rate was therefore determined to be 0.48 ± 0.085 W/K.

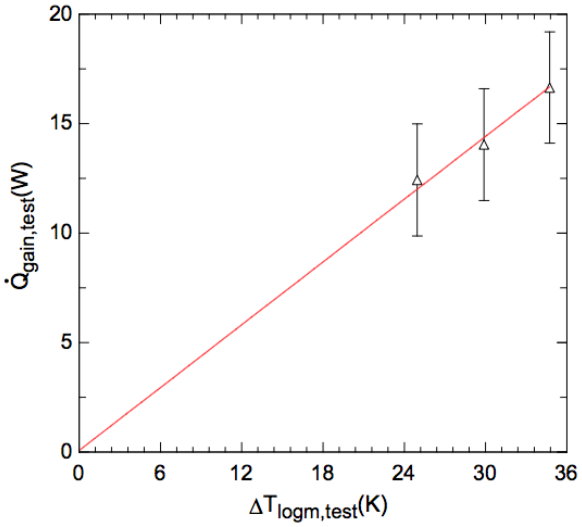

Figure 6. Determination of the thermal conductance of the test section at a fixed coolant mass flow rate

5. Estimation of experimental uncertainty

The uncertainty propagation analysis for the experimentally determined heat transfer coefficients and vapour qualities was performed using the Taylor Series Method. This relates the unknown error of calculated variables to the estimated error of measured quantities through the relationship,

$$U_Y = \sqrt{\sum_i \left(\frac{\partial Y}{\partial X}\right)^2 U_{X_i}^2} \tag{14}$$

Here, U_Y represents the unknown uncertainty of the calculated variables Y, and U_X is the uncertainty for the measured variables X, which include the measurements of the temperature, pressure, mass flow rate and the electrical input to the preheater. Original readings of thermocouples and pressure transducers from the data logger were calibrated against reference values to reduce reading errors. The uncertainty after the calibration for the temperature measurement was determined to be ±0.015 K for all thermocouples, and uncertainties for the pressure measurement were ±4 kPa, ±3 kPa and ±7 kPa for P_1, P_2 and P_3, respectively. The measurement uncertainty of the Coriolis mass flow meter was stated by the manufacturer to be ±0.1% of the measured flow rate. The measurement uncertainties of the real-time voltage and current applied to the preheater by the clamp meter were ±1.2% and ±1%. The uncertainty propagation analysis determined that the uncertainties in the experimental heat transfer coefficient varied between ±7.8% and ±23.7%, and that the uncertainty in the vapour quality was between ±1.6% and ±2.5%.

6. Experimental results and discussions

6.1 Prediction of the flow regime

Since the experimental test rig did not allow for the visual observation of the flow regimes of the CO_2 two-phase flow inside the test section, the flow regime of all measurement points was determined using the transition criteria proposed by Li and Norris [1]. This is based on the experimental observations by Jang and Hrnjak [4], and uses the value of the Soliman Froude number, Fr_{so}, with values of $Fr_{so} = 14$ and $Fr_{so} = 6$ signifying the transition from annular-to-wavy and wavy-to-stratified flow for CO_2 flow condensation in smooth tubes. In Fig.7, the experimental data points for this study are plotted in terms of mass flux and vapour quality, with the predicted flow regime being denoted by the symbol as ●: annular, ■: wavy, and ▲: stratified.

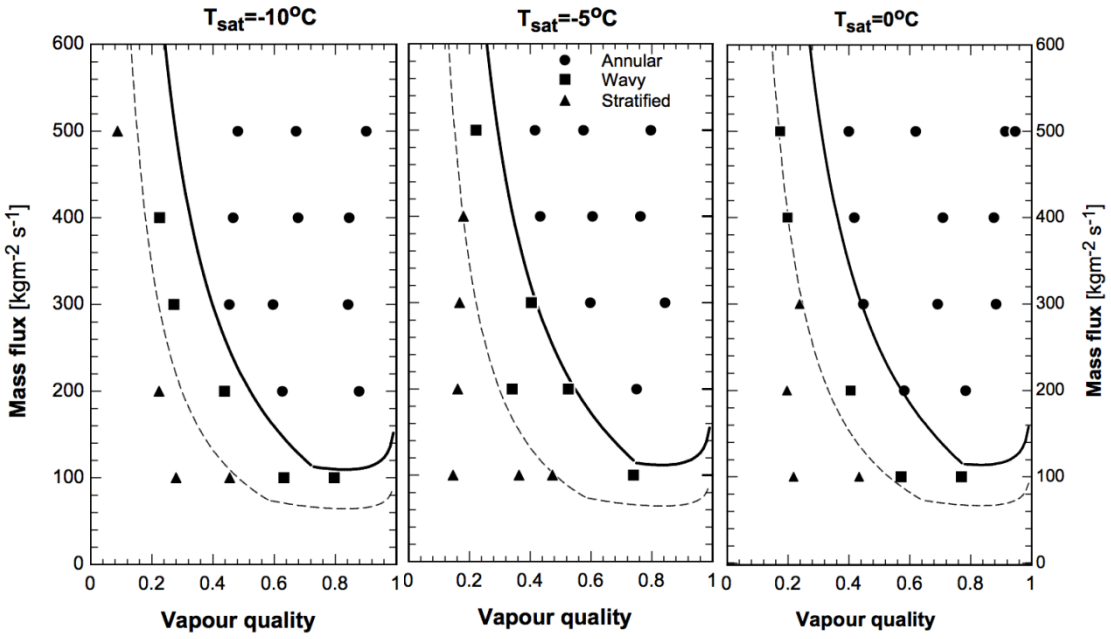

Figure 7. The flow regimes of the experimental data points, predicted with the Soliman Froude number [1] $Fr_{so} = 6$ (Dashed line) $Fr_{so} = 14$ (Solid line)

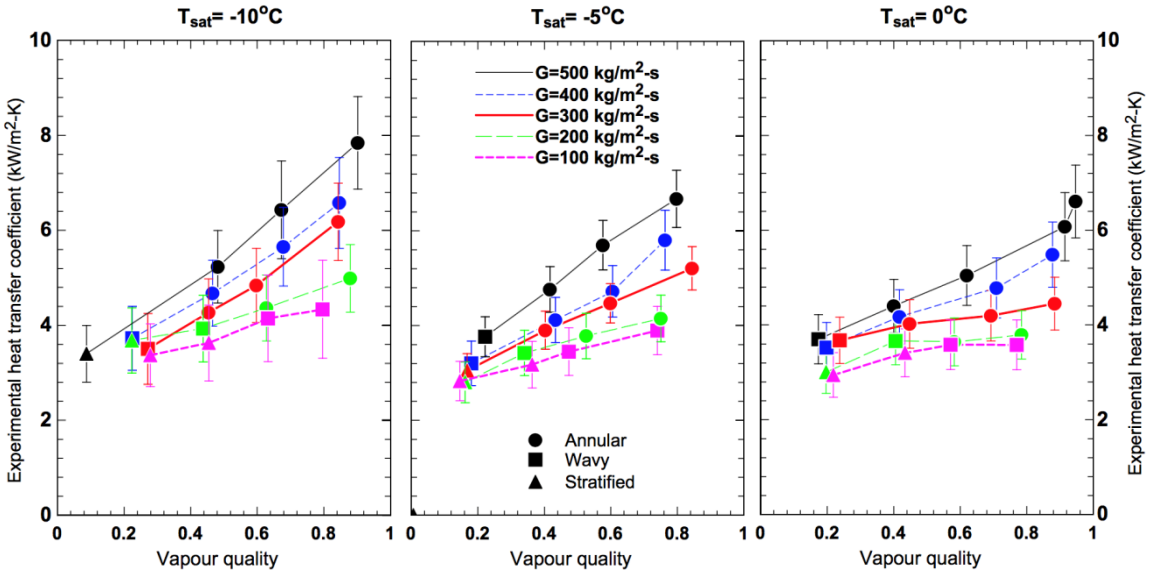

Figure 8. The experimental heat transfer coefficients for mass fluxes ranging from 100 to 500 kg/m^2-s under different saturation temperatures

6.2 Effects of mass flux and vapour quality on heat transfer

In Fig.8, the experimental heat transfer coefficients (HTCs) are plotted over the full range of vapour quality for mass fluxes ranging from 100 to 500 kg/m^2-s and saturation temperatures of -10°C, -5°C and 0°C. It can be seen that for all saturation temperatures, the HTCs increased with increasing mass flux and vapour quality. At low mass fluxes of 100 and 200 kg/m^2-s, the variation of HTC with increasing mass flux and vapour quality was moderate. For mass fluxes of 300 kg/m^2-s, when vapour qualities exceeded 0.4 the HTCs increased more significantly with increasing vapour quality. A similar trend was found for the higher mass fluxes of 400 and 500 kg/m^2-s, but occurred at a lower vapour quality of approximately 0.2. Therefore, it can be concluded that the dependence of the HTC upon vapour quality is weak for mass fluxes less than 300 kg/m^2-s, but is much stronger for mass fluxes above 300 kg/m^2-s. Quantitatively, under a saturation temperature of -5˚C, as the vapour quality increased from 0.2 to 0.8, HTCs increased by 71%, 81% and 77% for mass fluxes of 300, 400 and 500 kg/m^2-s, respectively. However, for mass fluxes of 100 and 200 kg/m^2-s, as the vapour quality increased from 0.2 to 0.8, HTCs only increased by 38% and 48%.

The flow regimes of the measurement points are illustrated with different symbols in Fig.8, corresponding to the predictions shown in Fig.7. It can be seen that the HTCs of the annular flow data points are much more strongly dependent on the mass flux and vapour quality than those for stratified flow. This trend agrees with the convective and film condensation mechanisms for annular and stratified flows discussed in Thome et al. [18]. In annular flow, the HTC is limited by the heat transfer rate through the annular layer of liquid condensate. An increase in the vapour quality reduces the thickness of the annular layer, and for a given vapour quality, an increase in the mass flux increases the velocity of the vapour, increasing the shear stress in the turbulent annular layer. In both cases, the effect is to increase the temperature gradient in the layer, thereby increasing the HTC. For stratified flow, the heat transfer is dominated by the conduction through the film of condensate on the upper surface of the tube. Due to the low two-phase velocities, the flow in the condensing film is dominated by gravity [19]. Therefore, variations in mass fraction and vapour quality have a lower effect than for annular flows. It should be noted that the hypothesis that these phenomena can be related to single-phase flow convection and Nusselt film condensation is not a new one, and is the basis for several successful models [19-21].

6.3 Effect of saturation temperature on heat transfer

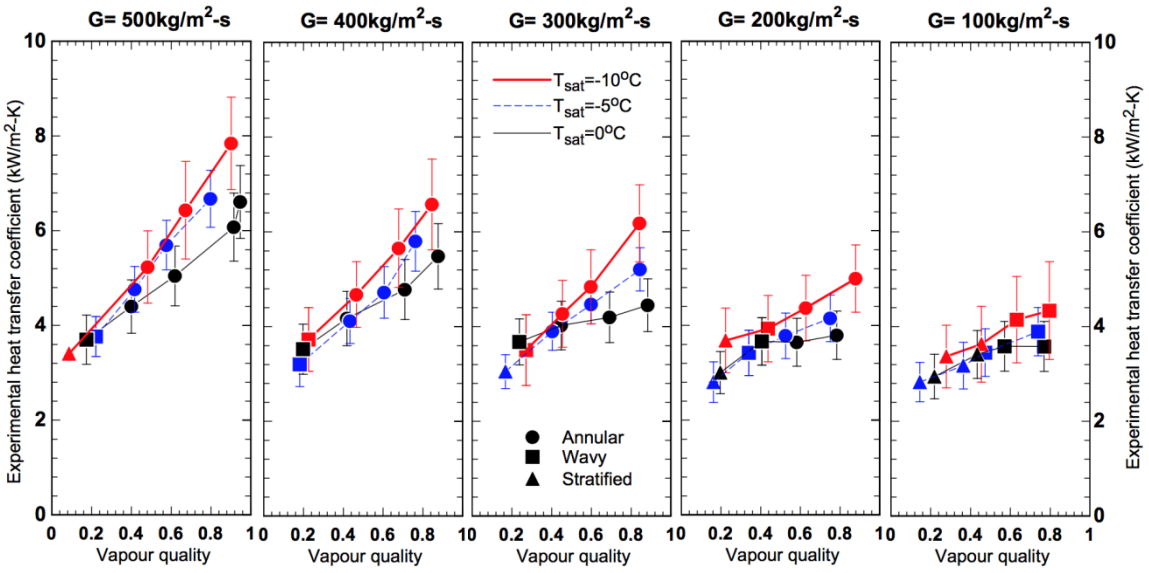

Figure 9. Experimental heat transfer coefficients at saturation temperatures of -10°C, -5°C and 0°C for different mass fluxes

The experimental HTCs at saturation temperatures of -10°C, -5°C and 0°C are plotted versus vapour quality for different mass fluxes in Fig.9. The general trend is that heat transfer increased with a decrease in the saturation temperature.

In Fig.9, the dependency of heat transfer on saturation temperature becomes greater with increasing mass flux. At low mass fluxes of 100 and 200 kg/m^2-s, for vapour qualities less than 0.6, heat transfer was insensitive to saturation temperature. But for high mass fluxes ranging from 300 to 500 kg/m^2-s, for vapour qualities less than 0.4 there was no apparent dependency upon saturation temperature. Using the predictions of the flow regime shown in Fig.9, it can be concluded that decreasing saturation temperature has a much more significant effect on the annular flow condensation than the stratified flow condensation.

Examining the effect of saturation temperature on the thermophysical properties of the refrigerant, the vapour density of CO_2 at -10°C and -5°C is 73% and 85% of the value at 0°C, respectively. For heat transfer in annular flows, for a given mass flux and vapour quality, the lower vapour density of CO_2 will result in a higher vapour velocity, and thus a higher vapour shear stress will be exerted on the liquid film. The mean velocity within the liquid film is increased and so the increased turbulence will lead to a higher heat transfer rate. For stratified flow, the property differences caused by the decreasing saturation temperature had a minor effect in determining the liquid film thickness, and so a minor effect on the HTC.

6.4 Predictions using the existing CO_2 flow condensation models

The specifically proposed flow condensation models for CO_2 by Heo and Yun [13], Shah [14] and Li and Norris [1] were evaluated against the current experimental data, and the comparison is shown in Fig.10. The Heo and Yun model under predicts the low Nusselt number data points, and over predicts the experimental results in the high Nusselt number range. The Shah model over predicts the data points at high Nusselt numbers, but it makes acceptable predictions for the low and medium Nusselt number data. The Li and Norris model predicts most of the experimental data points within ±20% but underpredicts the data at low Nusselt numbers.

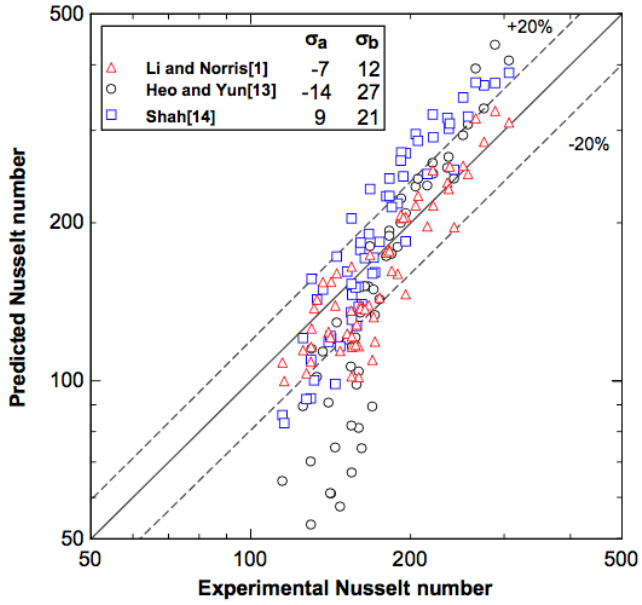

Figure 10. Comparison between the experimental heat transfer coefficients and predictions by CO_2 flow condensation models [1, 13, 14]

6.5 Modification to the Li and Norris flow condensation model

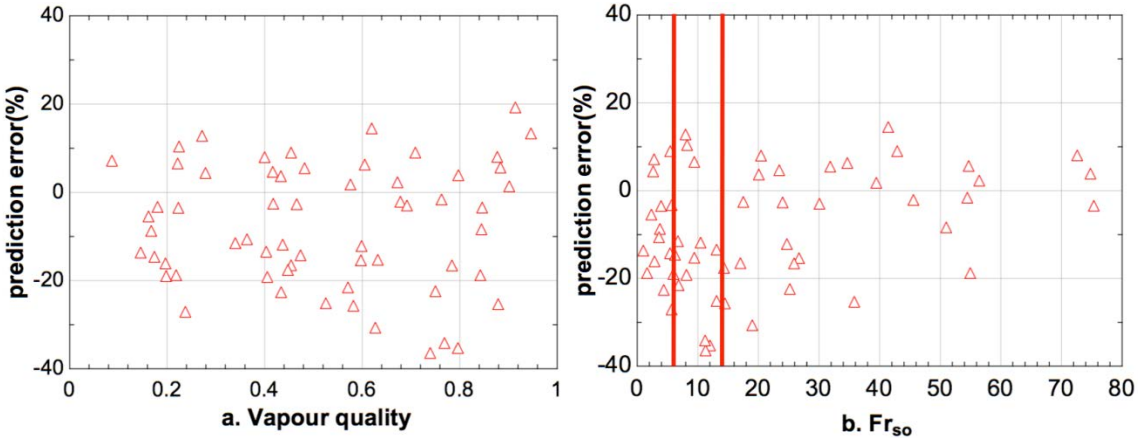

Figure 11. Prediction errors of the Li and Norris model versus a. vapour quality, and b. Soliman's modified Froude number Fr_{so}

In Fig.11a and 11b, prediction errors of the Li and Norris model are plotted versus vapour quality and Soliman's Froude number Fr_{so}. In Fig.11a, the data points with the highest prediction errors are seen to be concentrated between vapour qualities of 0.6 and 0.8. In Fig.11b, the transition values of $Fr_{so} = 14$ and $Fr_{so} = 6$, are highlighted with red lines. It can be seen that prediction errors over $Fr_{so} = 14$ are evenly distributed within ±20%. When $Fr_{so}$is approaching 14, errors start to increase, and the largest errors are approximately -40%. For Soliman Froude numbers less than 10, the Nusselt numbers are predicted within ±20%. This suggests that data points in the annular-to-wavy transition boundary are not correctly predicted by the Li and Norris model, and examination of the data showed that they were for mass fluxes of 100 and 200 kg/m^2-s.

The Li and Norris model calculated heat transfer through the annular-to-stratified transition by linear interpolation between the boundary values of annular ($Fr_{so} = 14$) and stratified ($Fr_{so} = 6$) flow heat transfer coefficient based on the actual Froude number. This procedure incorrectly predicted the wavy flow condensation data experimentally measured in this study. In addition, it incorrectly leads to a lower heat transfer coefficient at the end of annular flow than the start of stratified flow because of the interpolation procedure. Therefore, it was proposed to ignore the wavy regime, and transition the heat transfer mechanisms directly between the annular and stratified regimes.

In Fig.12, the annular and stratified flow heat transfer coefficients predicted by the Li and Norris model are plotted for the full vapour quality range, for mass fluxes ranging between 100 to 800 kg/m^2-s. For each value of mass flux, the predicted annular (solid line) and stratified (dashed line) heat transfer coefficients intersect (red dot), which corresponds to a vapour quality point x_{int}. These intersection vapour quality points can be used as the boundary values for transition from annular to stratified flow, with no interpolation through the wavy regime. The correlation between x_{int} and mass flux G was calculated to be,

$$x_{int} = 104288G^{-2.23} \tag{15}$$

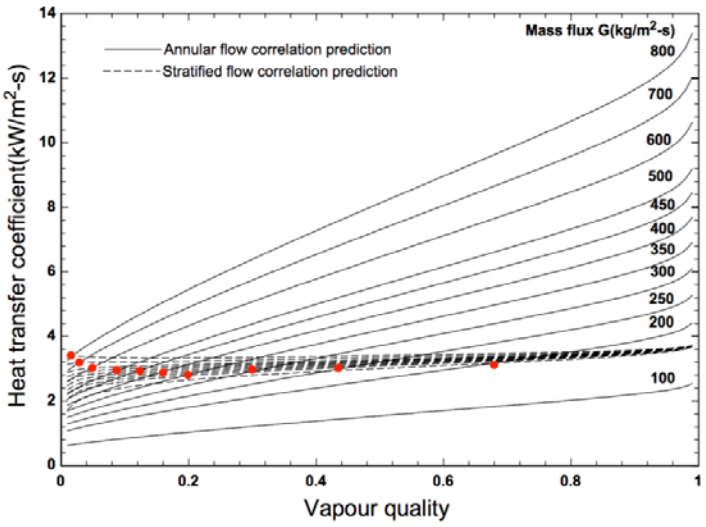

Figure.12 The heat transfer coefficients predicted by the Li and Norris model for stratified and annular flow

The modified Li and Norris model is given in Table.3.

Flow regime	Transition value	Heat transfer correlations
Annular	$x > 104288G^{-2.23}$	$D > 3mm, \quad a = 0.023\ b = 0.42\ c = 0.786$ $D < 3mm, \quad a = 0.02 \quad b = 0.54\ c = 1.61$ $h_a = \left(1 + \frac{1.2}{X_{tt}^{0.935}}\right) aRe_{ls}^{0.8} Pr_l^{0.4} \frac{k_l}{D}$
Stratified	$x \leq 104288G^{-2.23}$	$h_s = \frac{0.56}{1 + bX_{ll}^c} h_{film} + (1 - \theta_s/\pi)0.023Re_l^{0.8} Pr_l^{0.4} \frac{k_l}{D}$ $h_{film} = \left[\frac{\rho_l(\rho_l - \rho_v) g k_l^3 i_{lv}}{\mu_l D(T_{sat} - T_w)}\right]^{0.25}$ $\varepsilon = \frac{\varepsilon_h - \varepsilon_{ra}}{\ln(\varepsilon_h/\varepsilon_{ra})} \qquad \varepsilon_h = \left[1 + \left(\frac{1-x}{x}\right)\left(\frac{\rho_v}{\rho_l}\right)\right]^{-1}$ $\varepsilon_{ra} = \frac{x}{\rho_v}\left([1 + 0.12(1-x)]\left(\frac{x}{\rho_v} + \frac{1-x}{\rho_l}\right) + \frac{1.18(1-x)[g\sigma(\rho_l - \rho_v)]^{0.25}}{G\rho_l^{0.5}}\right)^{-1}$ $1 - \theta_s/\pi = \frac{\arccos(2\varepsilon - 1)}{\pi}$

Table.3 The modified model of Li and Norris [1] for CO_2 flow condensation heat transfer

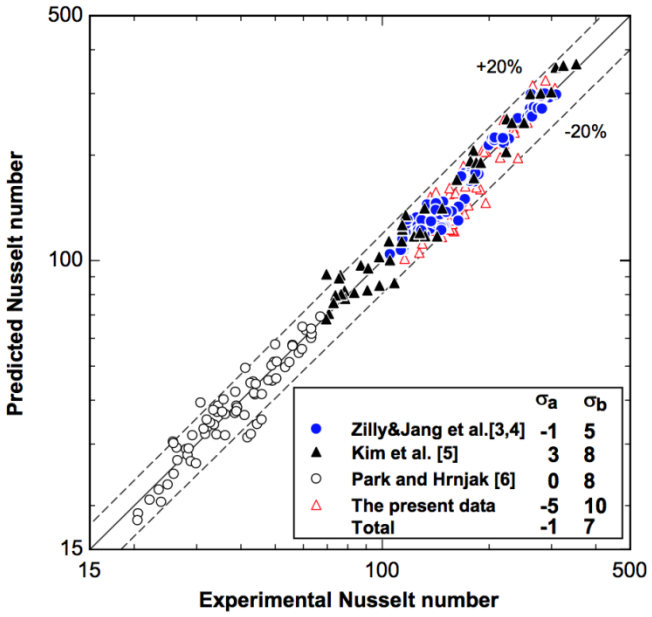

Figure.13 Comparison between the experimental data sets including Zilly et al. [3], Jang and Hrnjak [4], Kim et al. [5], Park and Hrnjak [6] and the current study, and predictions by the modified Li and Norris model.

A new data bank for in-tube flow condensation of CO_2 was created including the current experimental data, and the experimental data of Zilly et al. [3], Jang and Hrnjak [4], Kim et al. [5] and Park and Hrnjak [6]. The databank includes a total of 282 data points of CO_2 flow

condensation heat transfer with mass fluxes of 100 to 800 kg/m^2-s, at saturation temperatures of -25 to 0°C, inside tubes with inner diameter of 0.89 to 6.1 mm. Comparison between these experimental data points and the predictions by the modified Li and Norris model is shown in Fig.13. It exhibits a good agreement with the experimental data, having a mean absolute percentage deviation of 7%.

7. Conclusions

In this study, the heat transfer coefficient of CO_2 flow condensation inside a 4.73 mm inside diameter horizontal tube was measured for a wide range of vapour qualities, for mass fluxes of 100 to 500 kg/m^2-s, at saturation temperatures of -10, -5 and 0°C.

The experimental results showed that the dependency of the heat transfer coefficient upon vapour quality varied with mass flux. At low mass fluxes the heat transfer coefficient did not vary with vapour quality. However, at high mass fluxes the heat transfer coefficient increased linearly with increasing vapour quality. In addition, at low vapour qualities (less than 0.4) the heat transfer coefficient was approximately constant (between 3 and 4 kW/m^2-K) for all mass fluxes. These findings agree with the heat transfer mechanisms in the flow regimes of the experimental data.

For annular flows, a decrease in the saturation temperature increased the heat transfer coefficient. This was particularly true at higher mass fluxes. This phenomenon was due to the lower vapour density of CO_2 for low saturation temperatures.

Comparison between the current experimental data and existing flow condensation models for CO_2 showed that the Li and Norris model was the most accurate but under-predicted the heat transfer coefficient at low Nusselt numbers. An improved version of the Li and Norris model was developed that correctly predicts a total of 282 heat transfer data points, from this and other experimental studies, with a mean absolute percentage deviation of 7%.

Nomenclature

A	preheater current, A	X_{tt}	turbulent-turbulent Lockhart-Martinelli number
A_c	cross-sectional area, m^2	UA	heat conductance, W/K
D	diameter, m	V	preheater voltage, V
$\dot{E}$	electric power, W	***Greek symbols***	
Fr_{so}	Soliman's modified Froude number	u	velocity, m/s
Re_{ls}	superficial liquid Reynolds number, GD(1-x)/μ_l	μ	dynamic viscosity, kg/m-s
Re_{vs}	superficial vapour Reynolds number, GDx/μ_v	σ	surface tension, N/m
Re_l	the liquid Reynolds number, GD/μ_l	Θ	angle
c_p	specific heat at constant pressure, J/(kgK)	σ_a	the mean percentage deviation
G	mass flux, kg/(m^{2}s)	σ_b	the mean absolute percentage deviation
h	heat transfer coefficient, W/(m^{2}K)	***Subscripts***	
i	enthalpy, J/kg	amb	ambient
i_{lv}	enthalpy of vaporisation, J/kg		

I	preheater current, A	h	homogenous
k	thermal conductivity, W/(mK)	l	liquid
$\dot{m}$	mass flow rate, kg/s	$logm$	log-mean difference
P	Pressure, KPa	$gain$	heat gain
Pr	Prandtl number	pre	preheater
$\dot{Q}$	heat transfer rate, W	s	stratified
T	temperature, K	sat	saturation
R	thermal resistance, K/W	$test$	test section
x	vapour quality	v	vapour
X_{ll} number	laminar-laminar Lockhart-Martinelli	w	tube wall

References

1. Li, P. and S. Norris, *Heat transfer correlations for CO2 flowing condensation in a tube at low temperatures.* Applied Thermal Engineering, 2016. **93**: p. 872-883.
2. Pearson, S.F., *Using CO2 to reduce refrigerant charge.* ASHRAE Journal, 2012. **54**(10): p. 38-43.
3. Zilly, J., J. Jang, and P.S. Hrnjak, *Condensation of CO2 at low temperature inside horizontal microfinned Tubes.* Air-Conditioning and Refrigeration Center **CR49**. University of Illinois at Urbana-Champaign. 2003.
4. Jang, J. and P.S. Hrnjak, *Condensation of CO2 at low temperature.* Air-Conditioning and Refrigeration Center **CR56**. University of Illinois at Urbana-Champaign. 2004.
5. Kim, Y.J., J. Jang, P.S. Hrnjak, and M.S. Kim, *Condensation heat transfer of carbon dioxide inside horizontal smooth and microfin tubes at low temperatures.* Journal of Heat Transfer, 2009. **131**(2): p. 1-10.
6. Park, C.Y. and P. Hrnjak, *CO2 flow condensation heat transfer and pressure drop in multi-port microchannels at low temperatures.* International Journal of Refrigeration, 2009. **32**(6): p. 1129-1139.
7. Iqbal, O. and P. Bansal, *In-tube condensation heat transfer of CO2 at low temperatures in a horizontal smooth tube.* International Journal of Refrigeration, 2012. **35**(2): p. 270-277.
8. Heo, J., H. Park, and R. Yun, *Condensation heat transfer and pressure drop characteristics of CO2 in a microchannel.* International Journal of Refrigeration, 2013. **36**(6): p. 1657-1668.
9. Thome, J.R. and G. Ribatski, *State-of-the-art of two-phase flow and flow boiling heat transfer and pressure drop of CO2 in macro- and micro-channels.* International Journal of Refrigeration, 2005. **28**(8): p. 1149-1168.
10. Fang, X., Z. Zhou, and D. Li, *Review of correlations of flow boiling heat transfer coefficients for carbon dioxide.* International Journal of Refrigeration, 2013. **36**(8): p. 2017-2039.
11. Li, P., J.J.J. Chen, and S. Norris, *Review of flow condensation of CO2 as a refrigerant.* International Journal of Refrigeration, 2016. **72**: p. 53-73.
12. Kang, P., J. Heo, and R. Yun, *Condensation heat transfer characteristics of CO2 in a horizontal smooth tube.* International Journal of Refrigeration, 2013. **36**(3): p. 1090-1097.
13. Heo, J. and R. Yun, *Prediction of CO2 condensation heat transfer coefficient in a tube.* International Journal of Thermal Sciences, 2015. **89**(0): p. 254-263.
14. Shah, M.M., *Prediction of heat transfer during condensation of carbon dioxide in channels.* Applied Thermal Engineering, 2016. **93**: p. 192-199.

15. Cavallini, A., G. Censi, D. Del Col, L. Doretti, G.A. Longo, L. Rossetto, and C. Zilio, *Condensation inside and outside smooth and enhanced tubes — a review of recent research.* International Journal of Refrigeration, 2003. **26**(4): p. 373-392.
16. Shah, M.M., *A general correlation for heat transfer during film condensation inside pipes.* International Journal of Heat and Mass Transfer, 1979. **22**(4): p. 547-556.
17. Shah, M.M., *General correlation for heat transfer during condensation in plain tubes: further development and verification.* ASHRAE Transactions, 2013. **119**: p. 3.
18. Thome, J.R., J. El Hajal, and A. Cavallini, *Condensation in horizontal tubes, part 2: new heat transfer model based on flow regimes.* International Journal of Heat and Mass Transfer, 2003. **46**(18): p. 3365-3387.
19. Dobson, M.K. and J.C. Chato, *Condensation in Smooth Horizontal Tubes.* Journal of Heat Transfer, 1998. **120**(1): p. 193-213.
20. Shah, M.M., *An Improved and Extended General Correlation for Heat Transfer During Condensation in Plain Tubes.* HVAC&R Research, 2009. **15**(5): p. 889-913.
21. Cavallini, A., D.D. Col, L. Doretti, M. Matkovic, L. Rossetto, C. Zilio, and G. Censi, *Condensation in Horizontal Smooth Tubes: A New Heat Transfer Model for Heat Exchanger Design.* Heat Transfer Engineering, 2006. **27**(8): p. 31-38.